Published in final edited form as:

Conf Proc IEEE Eng Med Biol Soc. 2012 ; 2012: 594–597. doi:10.1109/EMBC.2012.6346001.

Towards Ultrahigh Throughput Microinjection: MEMS-based Massively-parallelized Mechanoporation

Yanyan Zhang,
Department of Mechanical Engineering, University of California, Riverside, CA 92521 USA, phone: 951-827-5871

Christopher B. Ballas, and
Research Assistant Professor with the Division of Hematology/Oncology, Indiana University School of Medicine, Indianapolis, IN 46202 USA

Masaru P. Rao [Member, IEEE]
Assistant Professor with the Department of Mechanical Engineering, University of California, Riverside, CA 92521 USA

Yanyan Zhang: yazhang@engr.ucr.edu; Christopher B. Ballas: cballas@iupui.edu; Masaru P. Rao: mprao@engr.ucr.edu

Abstract

We describe a massively-parallelized, MEMS-based device concept for passively delivering exogeneous molecules into living cells via mechanical membrane penetration, i.e., mechanoporation. Details regarding device design and fabrication are discussed, as are results from preliminary live cell studies focused on device validation at the proof-of-concept level. These efforts represent key steps towards our long-term goal of developing instrumentation capable of ultrahigh throughput (UHT) cellular manipulation via active microinjection.

I. Introduction

Microinjection is a well-established cellular manipulation technique that enables introduction of exogenous materials into a cell [1, 2]. As shown in Fig. 1, microinjection instrumentation typically requires an operator to first locate the cell to be manipulated and then capture it using aspiration (i.e. suction) from a micropipette attached to a manually-controlled micromanipulator. Using a separate micromanipulator, the operator then inserts a needle into the cell for injection, retracts the needle when completed, and releases the cell by reversing aspiration flow. This procedure is then repeated serially until sufficient numbers of cells have been manipulated for the desired application.

While microinjection is used widely in the engineering of cell lines, oocytes, and embryonic stem cells for transgenic animal generation and *in vitro* fertilization, its reliance upon skilled labor nonetheless limits its availability, since new operators typically require many months of training to develop proficiency. Moreover, the combination of manual operation and serialized injection methodology limits throughput (~3 cells/min), which constrains progress

in many current applications. Finally, these limitations have also precluded use of microinjection in other applications where it may hold considerable promise (e.g., *ex vivo* cell therapies, where microinjection may provide a safe, efficacious, and more precise alternative to bulk manipulation techniques, such as viral vectors, lipofection, and electroporation).

Recent efforts to automate the microinjection process by replacing the operator with robotics have shown promise for improving success rates [3–6]; however, this has come at the expense of instrument complexity. Moreover, only modest gains in throughput have been achieved (≤35 cells/min). Complementary efforts have sought to use MEMS fabrication techniques to create devices that improve injection reproducibility [6], or facilitate cell capture in ordered arrays for rapid identification and alignment [3–5, 7]. However, utility for ultrahigh throughput (UHT) microinjection continues to be limited by reliance upon serialized injection methodologies.

The true benefit of MEMS for microinjection lies in the promise for radically increasing throughput via massive parallelization. Fig. 2 illustrates one concept for realizing this promise, wherein cells are drawn onto an array of injectors by negative aspiration flow, injected, and then released from the array by positive aspiration flow. The monolithic integration of all functionalities within in a single chip enables considerable simplification relative to robotic serialized microinjection instrumentation, while massive parallelization offers opportunity for throughputs many orders of magnitude greater than the current state-of-the-art.

Herein, we describe development of an interim device that represents a key step towards UHT microinjection. In this device, the hollow injectors are replaced with solid penetrators. This simplifies device design and fabrication considerably, thus allowing expedited evaluation of key aspects of concept feasibility. Moreover, this design provides utility in and of itself, since it enables cellular manipulation via UHT mechanoporation, i.e. transient mechanical membrane disruption enables transfection via diffusive influx of exogenous molecules from the surrounding suspension.

II. Device Design

The UHT mechanoporation device consists of a 100 × 100 array of capture sites fabricated using bulk silicon micromachining. As shown in Fig. 3, each unit cell within the device is composed of a hemispherical capture site with monolithically integrated solid penetrator and aspiration vias. Capture site dimensions are dictated by the size of cells to be manipulated (K562 cells in this study). The aspiration vias provide connection to a common backside port to ensure uniformity of flow across the array. Elliptically-shaped vias are chosen to yield the desired well geometry and simplify fabrication. Use of multiple vias in each site provides uniform tension on the cell membrane to facilitate penetration. The penetrators are roughly conical with sub-μm tip and 1–2 μm base diameters, respectively. When coupled with the high strength of silicon, this maximizes reliability and minimizes penetration force, thus minimizing stress on the cell. Recent studies show that comparable structures produce

minimal membrane deformation, thus enhancing viability and reducing potential for mechanotransduction-induced artifacts [8, 9].

Aspiration flow rate requirements for cell capture and penetration are based upon earlier studies by Adamo and Jensen [10], which suggested need for cell velocities in excess of 1 mm/s to minimize membrane deformation during impingement upon microscale glass needles. For the UHT mechanoporation device, this corresponds to a global flow rate of 240 μL/min across the entirety of the capture site array. Assuming fully developed and steady Newtonian laminar flow, this produces an estimated pressure drop on the order of 1 kPa, based on analytical and numerical modeling. This is comparable to, or lower than other aspiration-based capture devices, none of which reported adverse effect on captured cells [4, 11, 12].

III. Device Fabrication

As shown in Fig. 4, the UHT mechanoporation device was fabricated using a silicon-on-insulator substrate with 20 μm device, 2 μm buried SiO_2 (BOX), and 500 μm handle layers. A 1 μm SiO_2 mask was first grown using wet oxidation, followed by an additional backside 2 μm SiO_2 deposition using plasma enhanced chemical vapor deposition. The aspiration vias were then lithographically patterned on the frontside and transferred into the SiO_2 mask by dry etching. Isotropic Si dry etching through the vias was then performed, resulting in simultaneous definition of both penetrator and capture well geometry in a single step. Once completed, Si deep reactive ion etching (DRIE) was performed to extend the Aspiration Vias to the BOX layer using the original oxide masking as a shadow mask. After removal of the frontside oxide masking via wet etching, the large aspiration ports were lithographically patterned and dry etched into the backside oxide mask, followed by extension to the BOX layer using DRIE. Finally, frontside dry etching was used to refine the penetrator tips to sub-μm dimensions, followed by removal of the BOX layer by dry etching.

IV. Mechanoporation studies

Preliminary device testing was performed using K652 cells. In most studies, Test samples were prepared in a single device operation cycle by: 1) pipetting 50k cells onto the device; 2) capturing cells via negative aspiration flow; 3) washing away uncaptured cells; 4) penetrating captured cells using a negative aspiration flow pulse; 5) releasing penetrated cells using positive aspiration flow; and 6) manually collecting released cells. Addition of propidium iodide to the collected cell suspensions enabled quantification of poration via flow cytometry. Also prepared were samples for: 1) Background – unstained cells collected directly from culture, centrifuged, and vortexed; 2) Negative Control - cells pipetted onto device surface, held quiescent for 1 min, collected, and then processed similarly to test samples; and 3) Positive Control - similar to background, but with addition of PI and NP40 detergent to disrupt the cell membranes. Overall device efficiency was estimated by subtracting poration efficiency of the Negative Control samples from the Test samples.

V. Results and Discussion

Scanning electron micrographs of a fabricated device are shown in Fig. 5. Realization of high-aspect-ratio, sub-μm tip diameter penetrators is clearly evidenced. However, capture well geometry deviates from the desired hemispherical profile, due to transport limitations during the isotropic etching step. Nevertheless, good uniformity of the capture sites is observed across the array.

Flow cytometry results from the live cell mechanoporation studies are shown in Fig. 6. Poration efficiency of ~15% is observed. While this is lower than desired, these data provide preliminary validation of the mechanoporation device concept. Moreover, we hypothesize that efficiency will be improved significantly in the near-future through implementation of pressure-based control for the aspiration circuit, rather than the current flow rate control approach. This hypothesis is based upon the observation that the capture site array is gradually populated during negative aspiration flow. This is suspected to subject captured cells to increasingly higher pressures as the array is populated, since flow rate through the remaining unpopulated capture sites must increase to meet the constant flow rate condition imposed on the aspiration circuit. Consequently, as pressure on the captured cells increases, potential for lysis increases as well, thus reducing poration efficiency. We are currently integrating an external pressure transducer within the aspiration circuit to test this hypothesis, and will use this as a means of implementing pressure-based control in the future.

VI. Conclusions

We report the design, fabrication, and testing of a MEMS-based device for cellular manipulation via massively parallelized mechanoporation. While low efficiencies are observed, preliminary validation of the device concept is demonstrated, thus representing a key step towards the ultimate realization of devices capable of UHT microinjection.

Acknowledgments

The authors thank the staff at the UC Riverside, UC Irvine, and UC Santa Barbara Nanofabrication Facilities for their assistance. The authors acknowledge support for this project under Grant# 8 R21GM0103973 from NIH/NIGMS.

References

1. Zhang Y, Yu LC. Single-cell microinjection technology in cell biology. Bioessays. Jun.2008 30:606–10. [PubMed: 18478541]
2. Zhang Y, Yu LC. Microinjection as a tool of mechanical delivery. Current Opinion in Biotechnology. Oct.2008 19:506–10. [PubMed: 18725294]
3. Cornell E, Fisher WW, Nordmeyer R, Yegian D, Dong M, Biggin MD, Celniker SE, Jin J. Automating fruit fly Drosophila embryo injection for high throughput transgenic studies. Review of Scientific Instruments. Jan.2008 79:013705. [PubMed: 18248037]
4. Sakai S, Youoku S, Suto Y, Ando M, Ito A. Automated high-throughput microinjection system for floating cells. Proc SPIE. Jan.2005 5699:59–65.
5. Wang W, Liu X, Gelinas D, Ciruna B, Sun Y. A fully automated robotic system for microinjection of zebrafish embryos. PloS ONE. Sep.2007 2:e862. [PubMed: 17848993]

6. Zappe S, Fish M, Scott MP, Solgaard O. Automated MEMS-based Drosophila embryo injection system for high-throughput RNAi screens. Lab on a Chip. Aug.2006 6:1012–9. [PubMed: 16874371]
7. Zhang X, Chen CC, Bernstein RW, Zappe S, Scott MP, Solgaard O. Microoptical characterization and modeling of positioning forces on Drosophila embryos self-assembled in two-dimensional arrays. J Microelectromech S. Oct.2005 14:1187–1197.
8. Nakamura C, Kamiishi H, Nakamura N, Miyake J. A nanoneedle can be inserted into a living cell without any mechanical stress inducing calcium ion influx. Electrochemistry. Aug.2008 76:586–589.
9. Obataya I, Nakamura C, Han S, Nakamura N, Miyake J. Nanoscale operation of a living cell using an atomic force microscope with a nanoneedle. Nano Letters. Jan.2005 5:27–30. [PubMed: 15792407]
10. Adamo A, Jensen KF. Microfluidic based single cell microinjection. Lab on a Chip. Aug.2008 8:1258–61. [PubMed: 18651065]
11. Fabienne R, Benoliel AM, Bongrand P. Aspiration of THP1 into a micropipette. Mechanical deformation of monocytic THP-1 cells: occurrence of two sequential phases with differential sensitivity to metabolic inhibitors. Experimental Biology Online. Feb.1997 2:1–14.
12. Seo J, Ionescu-Zanette C, Diamond J, Lal R, Lee LP. Integrated mulitple patch-clamp array chip via lateral cell trapping junctions. Appl Phys Lett. Mar.2004 84:1973–1975.

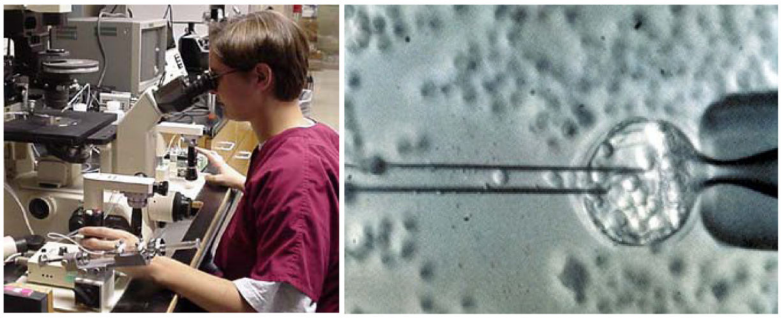

Figure 1.
Left: Conventional manual microinjection instrumentation. Right: Image of injection process from operator's perspective.

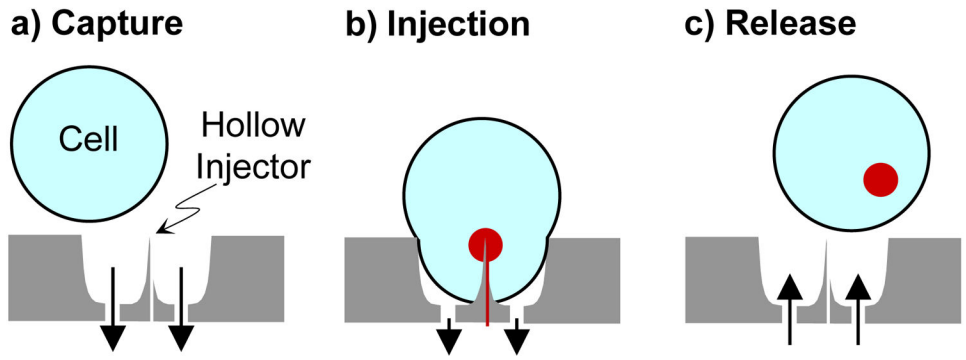

Figure 2.
MEMS-based UHT microinjection concept (illustrated for single capture site). Arrows denote flow direction and magnitude.

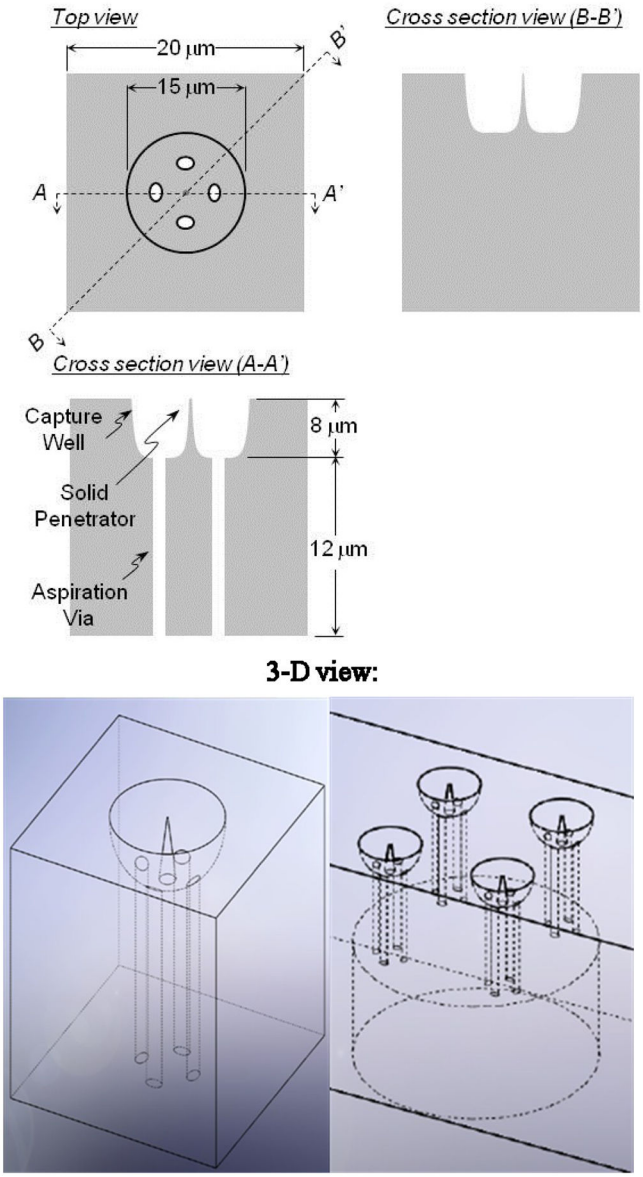

Figure 3.

Schematics of UHT mechanoporation device unit cell cross section views (top) and isometric views of single and multiple capture sites (bottom). In the latter, connection of multiple capture sites to a common backside aspiration port is illustrated. In actual devices, thousands of capture sites typically connect to each backside port.

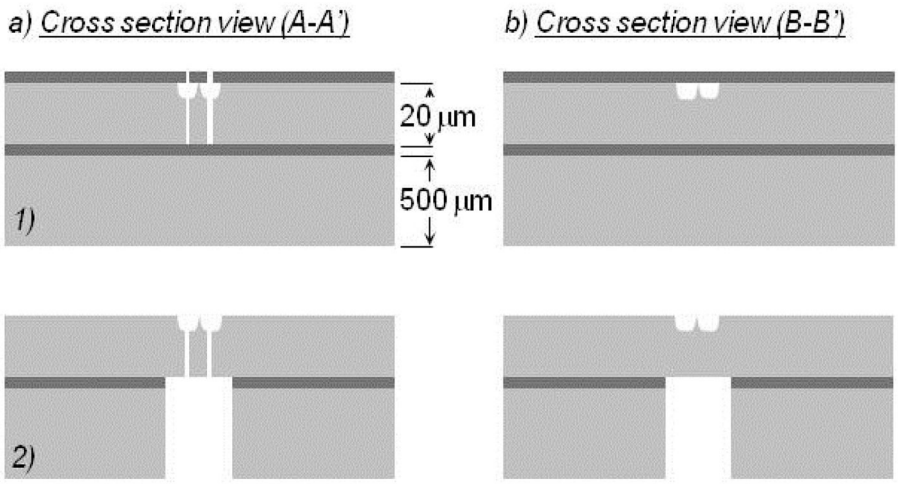

Figure 4.

Abridged fabrication process for UHT mechanoporation device. For the sake of clarity, only one capture site is pictured.

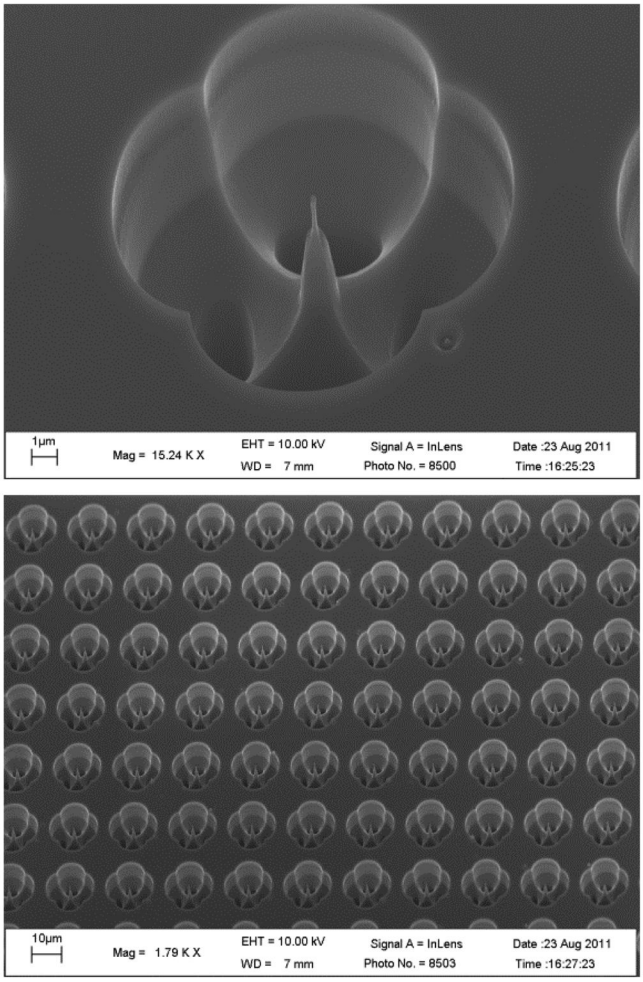

Figure 5.

Scanning electron micrographs of UHT mechanoporation device: (Top) Single capture site with ~200 nm tip diameter solid penetrator; and (Bottom) Lower magnification view of a portion of the 100 × 100 capture site array.

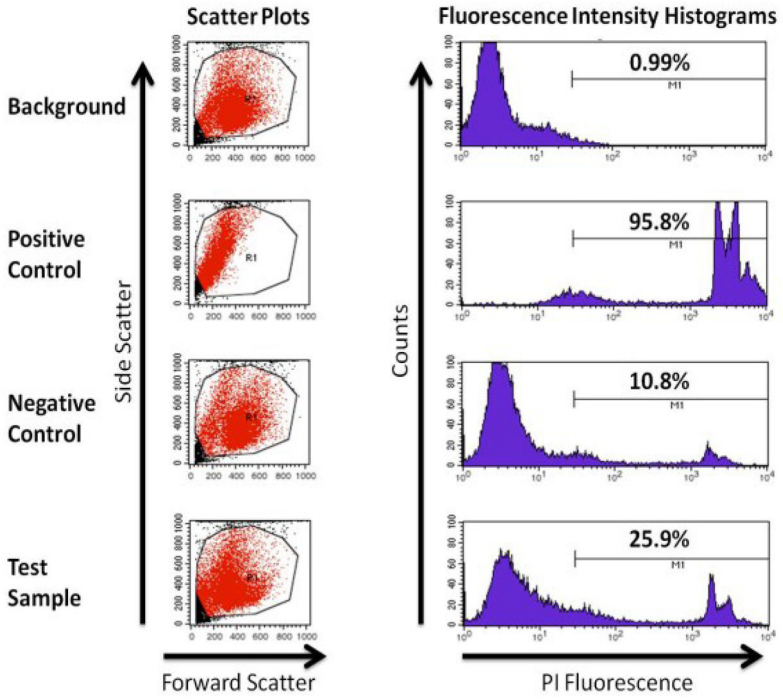

Figure 6.

Flow cytometry results for UHT mechanoporation device: (Left) Scatter plots (cell size/granularity) showing non-porated cells occupying larger population in center of plots and porated cells occupying population near side scatter axis; (Right) Histograms of cells pooled from 15 operation cycles showing overall poration efficiency of ~15% (percent dye positive cells indicated on each plot).